Pyroptosis Accelerates Spiral Ganglion Neuronal Degeneration Induced by Aminoglycosides in the Cochlea

Yazhi Xing (yazhi_0807@hotmail.com)
Department of otolayryngology, Shanghai Jiao Tong University Affiliated Sixth People's Hospital
https://orcid.org/0000-0001-8975-7242

Jia Fang
Department of Otolaryngology, Shanghai Jiao Tong University Affiliated Sixth People's Hospital

Zhuangzhuang Li
Department of Otolaryngology, Shanghai Jiao Tong University Affiliated Sixth People's Hospital

Mingxian Li
Shanghai Sixth People's Hospital: Shanghai 6th Peoples Hospital Affiliated to Shanghai Jiaotong University

Chengqi Liu
Department of Otolaryngology, Shanghai Jiao Tong University Affiliated Sixth People's Hospital

Xiaoxu Zhang
Department of Otolaryngology, Shanghai Jiao Tong University Affiliated Sixth People's Hospital

Yini Li
Department of Otolaryngology, Shanghai Jiao Tong University Affiliated Sixth People's Hospital

Song Mao
Department of Otolaryngology, Shanghai Jiao Tong University Affiliated Sixth People's Hospital

Haosong Shi
Department of Otolaryngology, Shanghai Jiao Tong University Affiliated Sixth People's Hospital

Kaiming Su
Department of Otolaryngology, Shanghai Jiao Tong University Affiliated Sixth People's Hospital

Dongzhen Yu
Department of Otolaryngology, Shanghai Jiao Tong University Affiliated Sixth People's Hospital
https://orcid.org/0000-0001-9424-4855

Haibo Shi
Department of Otolaryngology, Shanghai Jiao Tong University Affiliated Sixth People's Hospital

Research Article

Keywords: Neuroinflammation, pyroptosis, inflammasome, macrophages, ototoxicity, spiral ganglion neuron

Posted Date: December 28th, 2021

DOI: https://doi.org/10.21203/rs.3.rs-1158387/v1

Abstract

Background

In aminoglycoside-induced hearing loss, damage to spiral ganglion neurons (SGNs) accelerates gradually after the acute outer hair cell death, accompanied by macrophage infiltration and cytokine release. Pyroptosis plays a critical role in neurodegenerative diseases. Here, we explored the potential role of pyroptosis in SGN degeneration.

Methods

C57BL/6J mice were randomly divided into a kanamycin plus furosemide group and saline control group. Auditory functions were evaluated by auditory brainstem response tests conducted before treatment and at 1, 5, 15, and 30 days after treatment. HCs and SGNs were assessed for morphological alterations. SGNs were subjected to RNA sequencing and mRNA and protein analyses of NLRP3 inflammasome-related molecules. Macrophage activation was evaluated based on morphological and mRNA alterations. The effect of NLRP3 inhibition on SGN survival after kanamycin treatment was evaluated in organ explant cultures treated with Mcc950, a specific inhibitor of the NLRP3 inflammasome.

Results

Kanamycin and furosemide administration led to irreversible deterioration of the auditory brainstem response threshold, accompanied by acute loss of outer hair cells and gradually progressive loss of inner hair cells. SGNs showed a progressive decrease in quantity, as well as swelling and membrane rupture, at 15 and 30 days. RNA sequencing of SGNs showed that inflammation and immune-related responses were significantly upregulated, as was the expression of the inflammasome-related gene NLRP3. During 30 days of kanamycin exposure, the canonical pyroptosis pathway was constantly activated in SGNs. Activation and infiltration of microglia-like cells/macrophages, and increased production of cytokines, hallmarks of neuroinflammation, were also observed. Mcc950 significantly ameliorated SGN degeneration by inhibiting NLRP3 expression and promoting release of interleukins 1β and 18.

Conclusions

Pyroptosis causes cell death during aminoglycoside-induced SGN degeneration. Activation of the NLRP3 inflammasome leads to a cascade of inflammatory events in SGNs. Inhibition of the NLRP3 inflammasome significantly alleviates SGN damage, suggesting that it could serve as a new molecular target for the treatment of aminoglycoside-induced SGN degeneration.

Introduction

Ototoxic drug-induced hearing loss is one of the main types of hearing impairment. More than 600 chemicals with potential ototoxicity have been identified, including those commonly used in clinical practice [1]. Of these chemicals, aminoglycosides are of particular importance and widely employed because of their potent bactericidal activities and low bacterial resistance. There are nine Food and Drug Administration-approved aminoglycosides, of which kanamycin is commonly used for antibiotic-resistant bacterial infections. Despite their low cost and efficacy for the treatment of cystic fibrosis [2], renal dialysis [3], and multidrug-resistant tuberculosis [4], aminoglycosides have nonnegligible side effects. The ototoxic hearing loss induced by aminoglycosides affects millions of people worldwide [5, 6]. However, in some situations, the use of ototoxic antibiotics is unavoidable [7]. Of 63% of cases of hearing loss associated with aminoglycoside usage, 17% were attributed to genetic variations in mitochondrial DNA, including A1555G and C1494T [5, 8]. However, these mutations are somewhat rare [5, 9–14]. The mechanism underlying the vast majority of cases of aminoglycoside-induced deafness without mitochondria mutations has yet to be clarified.

According to previous studies, the damage caused by aminoglycosides begins at the base of the cochlea and progresses toward the apex, and it manifests mainly as a loss of outer hair cells (OHCs) and inner hair cells (IHCs) via inhibition of protein synthesis (which triggers intrinsic apoptosis). With advances in cochlear implant technology, thousands of patients with peripheral hearing loss can now hear sounds. However, efficacy varies widely; in this regard, neuronal survival is of particular importance, where survival and good function of spiral ganglion neurons (SGNs) are necessary for proper function of cochlear prosthetics. Several recent studies showed that SGN damage occurs simultaneously with, rather than as a retrograde damage after aminoglycoside-induced hair cell (HC) loss [15–17]. Furthermore, human temporal bone studies have suggested that SGNs can be affected by aminoglycosides even without the loss of HCs [18, 19]. Thus, it is critical to understand the biological effects of ototoxic insults on SGNs.

A large body of evidence suggests that apoptosis occurs in SGNs due to excessive reactive oxygen species levels and endoplasmic reticulum stress [20, 21] and to the loss of neurotrophic factors and excitatory inputs caused by HC ablation [22, 23]. SGNs progress through various prosurvival/proapoptotic stages and are a heterogenous population of both viable and dying cells [24]. The infiltration of macrophages/microglia-like cells suggests that a defensive immune response occurs in SGNs after aminoglycoside injury [25]. Several studies have reported increased expression of interleukin (IL)-1β, a proinflammatory cytokine, in cochleae after damage [26–30], although no studies have discussed the origin or effects of the released cytokines.

Non-inflammatory apoptosis cannot fully explain the sustained (lasting several months) and severe biological processes that ensue after even a single dose of aminoglycosides. In contrast to the non-inflammatory process of cell death, pyroptosis involves activation of pattern recognition receptors (PRRs) by damage-associated molecular pattern (DAMP) and pathogen-associated molecular pattern molecules, as well as the assembly of inflammasomes, activation of inflammatory caspases and Gasdermin D (GSDMD), and release of IL-1β and IL-18 [31–33]. The inflammasomes were composed of PRRs and caspase proteases with or without apoptosis-associated speck-like protein containing a CARD (ASC) [34].

PRRs mainly include NLRP3, NLRP1, NLRC4, and AIM2. In the central nervous system of amyotrophic lateral sclerosis patients, increased expression of NLRP3 was observed in astrocytes in association with the neuroinflammatory response [35]. Several studies have demonstrated accumulation of inflammasomes in neuronal cells, which contributes to the cell death induced by pyroptosis in Alzheimer's disease [36], Parkinson's disease [37], and traumatic brain injury [38, 39].

Based on these known functions of pyroptosis, along with the accumulation of inflammasomes observed in neurodegenerative diseases and the SGN damage and macrophage activation seen in cochleae after aminoglycoside administration, we postulate that activation of inflammatory caspases and inflammasomes plays an important role in SGN damage. We evaluated morphological and molecular changes in SGNs after kanamycin treatment, investigated the effects of pyroptosis on neuronal injury, and revealed the mechanisms underlying neuroinflammation in SGNs. Our results indicate that pyroptosis plays an important role in aminoglycoside-induced progressive SGN degeneration, and that inhibition of the NLRP3 inflammasome can significantly alleviate SGN damage; thus, targeting pyroptosis has potential for the treatment of aminoglycoside ototoxicity.

Materials And Methods

Animals

Adult C57BL/6J mice (age, 6–8 weeks; weight, 16–25 g) were used in the experiments. The mice were maintained under standard laboratory conditions (22 ± 1°C and 12 h/12 h dark/light cycle). All experimental protocols were approved by the Animal Ethics Committee of Shanghai Jiao Tong University Affiliated Sixth People's Hospital.

Mouse model

The animals were randomly divided into two groups. Mice in the experimental group were given 1 g/kg kanamycin sulfate (Sigma-Aldrich, St. Louis, MO, USA) subcutaneously; 0.4 g/kg (10 mg/ml) furosemide (H31021063; Shanghai Harvest Pharmaceutical Co., Ltd., Shanghai, China) was injected intraperitoneally 30 min later. Mice in the experimental group were randomly divided into 1-, 5-, 15-, and 30-day kanamycin treatment groups (1 D, 5 D, 15 D, and 30 D, respectively). The age-matched mice in the blank control (Con) group were injected with the same dose of saline subcutaneously or intraperitoneally.

Auditory brainstem response (ABR) test

The ABR test was performed using a sound system from Tucker-Davis Technologies (Alachua, FL, USA) before and 1, 5, 15, and 30 days after kanamycin injection in a soundproof chamber. The mice were anesthetized by intraperitoneal injection of 1% sodium pentobarbital (70 mg/kg), and their body temperature was maintained at approximately 37°C using a thermostatic heating pad. The recording electrodes were placed under the skin at the vertex of the skull, and the reference electrode and ground electrodes were positioned on either side of the mastoid. The electrostatic speaker was positioned

approximately 10 cm in front of the animals' ears. The auditory stimuli were tone bursts (tone frequency, 21.1/s; rise/fall time, 0.5 ms; duration, 10 ms; sampling rate, 200 kHz). The ABR evoked potential was amplified 20 times using an RA16 preamplifier (Tucker–Davis Technologies) and then collected (bandpass filter, 300–3,000 Hz; averaged 1,000 times; sampling rate, 25 kHz). Thresholds were measured at 4, 8, 16, 32, and 40 kHz. The stimulus intensity started at 90 dB sound pressure level (SPL) and was gradually decreased (in 5-dB increments) to 10 dB SPL. The final intensity before the disappearance of wave III from the ABR waveform was defined as the hearing threshold. A threshold of 95 dB SPL was assigned when the animal showed no response to stimuli at 90 dB SPL.

Organotypic culture of cochlear SGNs and Mcc950 treatment

The organ of Corti and SGNs were collected from postnatal day 3 C57BL/6J mice, dissected out and placed on a small amount of rat tail collagen gel (10 μl) in a cell culture dish, and incubated in Dulbecco's modified Eagle's medium/F12 (DMEM/F12; Gibco, Life Technologies, Carlsbad, CA, USA) supplemented with B-27 (Gibco), N-2 supplement (Gibco) and ampicillin (Sangon Biotech, Shanghai, China), which was conducted at 37°C in a cell incubator under a 5% CO_2 atmosphere. On the following day, fresh culture medium containing 1 mM kanamycin (Sigma-Aldrich) was added, alone or with 10 μm Mcc950 (MedChemExpress, Monmouth Junction, NJ, USA), for 24 h.

Cochlear immunofluorescence

The cochleae were removed from the temporal bone in ice-cold phosphate-buffered saline (PBS). After the stapes removed, the oval and round windows were opened, and a small hole was drilled in the cochlear apex. We rapidly infused 4% paraformaldehyde (Sangon Biotech) into the cochleae, which were kept at 4°C for 2 h. Then, the cochleae were decalcified using ethylenediaminetetraacetate (EDTA) solution (Sangon Biotech) until they became soft. Cochleae were embedded in optimal cutting temperature compound (Sakura Finetek, Torrance, CA, USA) and frozen at −80°C and then cryosectioned into 30-μm slices (to observe macrophages) and 10-μm slices (to observe SGN) using a cryostat (CM1860; Leica, Wetzlar, Germany). Sections containing apical, middle, and basal SGNs were used in the following experiment. For HC counting and macrophage imaging, basilar membranes with SGNs were dissected. The membranes and frozen slices were permeabilized using 1% TritonX-100 for 1 h, incubated in 10% goat serum for 1 h at room temperature, and incubated with primary antibodies at 4°C overnight. Subsequently, the samples were incubated with secondary antibodies for 2 h at room temperature after washing with PBS. Tissues were mounted with histology mounting medium containing DAPI (Sigma-Aldrich); images were then acquired using a confocal microscope (LSM 710; Zeiss, Oberkochen, Germany) and collected as a Z-stack. The primary antibodies included rabbit anti-myosin VIIa (1:200; Proteus Biosciences, Ramona, CA, USA), rabbit anti-GSDMD (1:100; Abcam, Cambridge, UK), mouse anti-NeuN (1:200; Abcam), rabbit anti-IBA-1 (1:500; Wako, Richmond, VA, USA), and rabbit anti-beta-III tubulin (1:300; Abcam). The secondary antibodies included Alexa Fluor 488 goat anti-rabbit IgG (H + L) (1:1,000; Invitrogen, Waltham, MA, USA), Alexa Fluor 555 goat anti-mouse IgG (H + L) (1:1,000; Invitrogen) and Alexa Fluor 555 goat anti-rabbit IgG (H + L) (1:1,000; Invitrogen). We used ImageJ software (National

Institutes of Health, Bethesda, MD, USA) to process the images, on which IHCs, OHCs, SGNs, and macrophages were counted. To avoid bias, analyses were conducted by an investigator blinded to the sample numbers.

Macrophage morphological analysis

ImageJ was used to quantify the total branch length and soma area of the macrophages. Briefly, seven to twelve frozen sections from three animals were collected in each subgroup and stained with an IBA-1 antibody. Then, we used the polygon selection tool of ImageJ to calculate the soma areas of macrophages and the segmented line tool to calculate the total branch length of every macrophage in the middle turn.

Cochlear hematoxylin and eosin (H&E) staining and immunohistochemistry

Decalcified cochleae were paraffin-embedded and serially sectioned (3 μm). For H&E staining, sections were dewaxed in a series of xylene and ethanol. The sections were then stained with H&E solution. For immunohistochemistry, the frozen sections were dried at room temperature and heated in a microwave at 37°C for 5 min. After washing three times with 0.1 M PBS, the sections were immersed in 0.4% pepsin for 15 min at 37°C, incubated with 3% hydrogen peroxide solution to block endogenous peroxidase for 25 min at room temperature, and blocked with 3% bovine serum albumin for 30 min. Next, the sections were incubated with primary antibodies (rabbit anti-NLRP3 antibody, 1:50; Cell Signaling Technology, Beverly, MA, USA; rabbit anti-Caspase-1 antibody, 1:300; Servicebio, Wuhan, China; rabbit anti-ASC antibody, 1:200; Proteintech, Rosemont, IL, USA; rabbit anti-IL-1β antibody, 1:200; Servicebio; rabbit anti-IL-18 antibody, 1:50; ABclonal, Woburn, MA, USA) overnight at 4°C. Secondary HRP-labeled goat anti-rabbit antibody (1:200; Servicebio) was added to the sections for 50 min, and diaminobenzidine was used to measure immunoreactivity.

Transmission electron microscopy (TEM)

The mice were transcardially perfused with 50 ml 0.1 M PBS and 50 ml 4% paraformaldehyde containing 2.5% glutaraldehyde while under deep anesthesia. Then, we collected the cochleae, removed the stapes, opened the oval and round windows, drilled a small hole in the cochlear apex, and perfused the cochleae with the above-described fixative solution. The cochleae were immersed in the solution overnight at 4°C. The next day, after rinsing with 0.1 M PBS three times, the cochleae were decalcified with EDTA solution until soft. The cochleae were post-fixed in 1% osmium tetroxide solution and maintained at 4°C for 2 h, without direct exposure to light. The cochleae were then dehydrated in 25%, 50%, 70%, 90%, 95%, and 100% ethanol (15 min for each concentration) at 4°C, followed by dehydration in acetone for 15 min at room temperature (three times). Next, the cochleae were embedded in Epon medium containing Eponate 812, dodecenyl succinic anhydride, nadic methyl anhydride and dimethyl aminophenol and cured in a 60°C oven. Ultrathin (70-nm) sections were cut using an ultramicrotome (RM2145; Leica) and then stained with 3% uranyl acetate and 0.5% lead citrate. Finally, ultrastructural images were acquired using a transmission electron microscope (Talos L120C; Thermo Fisher Scientific, Waltham, MA, USA).

RNA sequencing

Eighteen cochleae were subjected to RNA sequencing (RNA-seq) (six each from the Con, 1 D, and 15 D groups). SGNs were dissected out for total RNA extraction using Trizol reagent (Invitrogen) following the manufacturer's procedure. The quantity and purity of the RNA from triplicate samples from each group were analyzed using the 2100 Bioanalyzer and RNA 6000 Nano LabChip Kit (Agilent, Santa Clara, CA, USA). After purification, a final cDNA library of each sample was prepared using TruSeq RNA Sample Preparation v2 (Illumina, San Diego, CA, USA) in accordance with the manufacturer's protocol. Paired-end sequencing of 300 ± 50 bp paired-end reads was performed using the Illumina NovaSeq 6000 instrument at LC Sciences (Hangzhou, China). FastQC and RSeQC were used to verify the quality of the sequencing. We aligned reads to the published genome (ftp://ftp.ensembl.org/pub/release-101/fasta/mus_musculus/dna/) using HISAT2. The mapped reads were assembled by StringTie. Then, all transcriptomes were merged using a Perl script. After generating the final transcriptome, StringTie was used to calculate the fragments per kilobase of transcript per million reads sequenced, and differentially expressed mRNAs and genes based on a fold change ≥ 2 or ≤ 0.5 and p-value < 0.05 were identified using the edgeR package. Gene Ontology (GO) and Kyoto Encyclopedia of Genes and Genomes (KEGG) enrichment analyses, along with gene set enrichment analysis (https://www.broadinstitute.org/gsea/), were performed.

Western blot analysis

We collected SGNs from the cochleae of mice in each group and immersed them in pre-chilled 0.1 M PBS. Then, the tissues were homogenized in RIPA lysis buffer (Shanghai Epizyme Biomedical Technology Co., Ltd) containing a protease inhibitor and phosphatase inhibitor (Shanghai Epizyme Biomedical Technology Co., Ltd). The homogenate was centrifuged at 12,600 × *g* for 20 min in a centrifuge pre-cooled to 4°C. The supernatant was collected to determine the protein concentration using a bicinchoninic acid kit (Shanghai Epizyme Biomedical Technology Co., Ltd). Protein samples (30 μg) were separated by 4–12% sodium dodecyl sulfate–polyacrylamide gel electrophoresis and transferred onto 0.45-μm nitrocellulose membranes. The membranes were blocked with 5% non-fat milk for 1 h at room temperature on a shaking table. After blocking, the membranes were incubated with primary antibodies at 4°C overnight. After three washes with 1 × Tris-buffered saline containing Tween, the membranes were incubated with the appropriate secondary antibodies for 1 h at room temperature. Finally, signals were detected using a chemiluminescence imaging system (ChemiDoc XRS+ System; Bio-Rad, Hercules, CA, USA) and an enhanced chemiluminescence substrate (Shanghai Epizyme Biomedical Technology Co., Ltd). The bands were analyzed using ImageJ.

The following antibodies were used for western blot analysis: rabbit anti-NLRP3 (1:1,000; Cell Signaling Technology), mouse anti-Caspase-1 (1:200; Santa Cruz Biotechnology, Santa Cruz, CA, USA), rabbit anti-GSDMD (1:1,000; Abcam), mouse anti-ASC (1:200; Santa Cruz Biotechnology), rabbit anti-actin (1:5,000; Abcam), goat anti-rabbit secondary antibody (1:5,000; Sangon Biotech), and goat anti-mouse secondary antibody (1:5,000; Sangon Biotech).

Quantitative real-time polymerase chain reaction (qRT-PCR)

Total RNA was extracted from the samples using the EZ-press RNA Purification Kit (EZBioscience, Roseville, MN, USA) and subjected to reverse transcription using 4× Reverse Transcription Master Mix (EZBioscience) at 42˚C for 15 min followed by 95˚C for 30 s. qRT-PCR was performed using 2× SYBR Green qPCR Master Mix (EZBioscience) on the LightCycler 96 system (Roche, Mannheim, Germany). mRNA expression was normalized to the housekeeping gene *Gapdh* and calculated relative to the expression in the Con group using the comparative Ct method. Three replicates were performed for each assay, and each experiment was repeated at least three times. The primer sequences used in the experiment are listed in Table 1.

Enzyme-linked immunosorbent assay (ELISA) for IL-1β and IL-18

Commercial mouse ELISA kits (Cloud-Clone Corp., Wuhan, China) were used to quantify IL-1β and IL-18 expression in the cochlear SGNs, and cultured organ explants according to the manufacturer's instructions. We obtained SGN tissues from the cochleae of two mice in each group on the same day, lysed them using lysate (Cloud-Clone Corp), and collected the supernatant. For the in vitro experiment, four organ explants were assessed per group. Each experiment was repeated three times.

Statistical analyses

All values are expressed as means ± SEM. Two-way analysis of variance (ANOVA) was used to compare the ABR data among the groups at various time points. One-way ANOVA followed by Dunnett's post hoc test was used for the other analyses. All of the analyses were performed using SPSS software (version 26.0; SPSS Inc., Chicago, IL, USA). A p-value < 0.05 was taken to indicate statistical significance.

Results

Loss of auditory function and HCs after kanamycin treatment

To evaluate auditory function, ABR tests were performed before and 1, 5, 15, and 30 days after kanamycin administration (Fig. 1a). The thresholds were lifted to 81.67 ± 1.67, 76.67 ± 1.05, and 90.83 ± 1.54 dB SPL at 8, 16, and 24 kHz, respectively, in the 1 D compared with Con group (all p < 0.001). At 4, 32 and 40 kHz, no reaction to sound was detected, even with the most intense stimulus. The loss of function was irreversible; no recovery was noted after 5, 15, or 30 days. To further investigate HC alterations, myosin VIIa was used to visualize the cell structures on whole-mount basilar membranes (Fig. 1b). The extent of HC loss was similar to that reported in previous studies, with a rapid reduction seen in OHCs and a relatively gradual reduction in IHCs (Fig. 1c).

SGN degeneration after kanamycin administration

To investigate SGN alterations, NeuN staining was used to visualize cell structures in the cross-section. No obvious SGN loss was observed after 1 day, but the number of SGNs began to decrease on day 5. SGN loss was more profound in the basal than apical turn (Fig. 2a). After 15 and 30 days, only 87.0% and 63.8% of the SGNs remained in the middle turn of Rosenthal's canal, respectively (Fig. 2c). At each time point, cochleae from at least three animals were collected for H&E staining, and two were collected for TEM analysis. The space between the densely packed SGNs and surrounding satellite cells began to increase after 1 day (Fig. 2b). Similarly, the gap between the SGNs and satellite cells increased; moreover, the myelin sheath was broken, bubbles appeared in the cytoplasm and cell membrane, and organelles spilled out (as revealed by TEM). After 5 days, several SGNs showed an irregular membrane and swelling of the cell body, although the nuclei remained relatively normal; the condensing and wrinkling effects seen in apoptosis were not observed (Fig. 2b). Membrane rupture, which is a sign of pyroptosis, was identified in TEM images taken at 5 and 15 days. Bubbles and protrusions were discovered after 15 and 30 days on cross-sectional views of the cochleae. SGNs that were swollen, showed protrusion, or lacked membrane integrity were counted. The number of these abnormal SGNs increased gradually over 30 days (Fig. 2c), indicating that non-apoptotic cell death may have occurred during SGN degeneration.

Inflammation and the immune response were elevated in SGNs after kanamycin treatment

The SGNs were collected from the Con, 1 D, and 15 D groups for RNA-seq analysis. Differentially expressed genes (DEGs) are shown in Fig. 3a. There were 406 DEGs in the 1 D vs. Con and 15 D vs. Con group comparisons, suggesting that kanamycin induced changes in gene expression. A further 122 DEGs were observed in the 1 D vs. Con, 15 D vs. Con, and 1 D vs. 15 D group comparisons, as shown in the Venn diagram in Fig. 3b. GO enrichment analysis showed that the DEGs between the 1 D and Con groups were significantly enriched in the following pathways: immune system process, innate immune response, inflammatory response, and immune response (Fig. 3c). The genes associated with these biological processes remained at high levels after 15 days. KEGG pathway analysis showed that cytokine–cytokine receptor interaction, tumor necrosis factor (TNF) signaling, NOD-like receptor signaling, and chemokine signaling (associated with inflammation) were significantly enriched pathways in the 1 D vs. Con group comparison (Fig. 3d). Furthermore, according to a heatmap of the genes involved in the NOD-like receptor signaling pathway, combined administration of kanamycin and furosemide activated pyroptosis-related proteins, such as *Nlrp3*, *IL-1β*, *caspase-1* and *ASC*, which are also related to inflammation and the immune response (Fig. 3e).

Pyroptosis contributed to SGN degeneration after kanamycin-induced ototoxicity

Previous studies have shown that the NLRP3 inflammasome plays critical roles in the central nervous system, especially in the context of neurodegenerative diseases. In our model, the mRNA levels of *Nlrp3*, *ASC*, and *caspase-1* were all elevated and reached their highest levels on day 5 (Fig. 4a). Interestingly, after 30 days, the transcriptional levels of these key proteins in the pyroptosis pathway remained higher than in the Con group ($p < 0.01$). Immunoblotting confirmed that NLRP3, ASC, and caspase-1 expression increased significantly after 5 days and remained at high levels after 30 days, suggesting activation of

the pyroptosis pathway (Fig. 4b, 4c). The increased levels of NLRP3, ASC, and caspase-1 after 1 and 15 days were confirmed by immunohistochemical staining (Fig. 4d). Taken together, these results indicated marked canonical pyroptosis pathway activation. Moreover, *GSDMD* transcription increased sharply after kanamycin exposure, peaking at 5 days and declining thereafter (but remaining higher than in the Con group; Fig. 4a). We further analyzed the protein levels of the N-terminal fragment of GSDMD (N-GSDMD) and intact GSDMD and confirmed that their levels increased gradually over time, peaking at 30 days (Fig. 4c). Immunofluorescence staining revealed GSDMD accumulation in the SGN membrane after kanamycin administration (Fig. 4e). Furthermore, qRT-PCR showed that *Tlr2* and *Myd88* expression levels were significantly increased after kanamycin treatment (Supplementary Fig. S1).

Increased release of IL-1β and IL-18 contributed to neuroinflammation in SGNs

The effects of inflammasome activation included shearing and the release of IL-1β and IL-18. Regarding changes in effector cytokines during kanamycin-induced SGN degeneration, the mRNA levels of *IL-1β* and *IL-18* increased sharply after 1 day of kanamycin exposure and decreased thereafter (Fig. 5a). The increased expression of IL-1β and IL-18 seen at 1 and 15 days was confirmed by immunohistochemistry (Fig. 5b). Moreover, ELISA showed that the IL-1β protein level peaked after 5 days of kanamycin exposure and then gradually decreased, while IL-18 expression peaked after 15 days of treatment (Fig. 5c). In both cases, the levels did not decrease to those of the Con group. In summary, IL-1β and IL-18 were released after kanamycin administration, and were involved in the process of SGN neuroinflammation.

Macrophage activation and infiltration after kanamycin-induced SGN degeneration

As the primary cells sensing environmental changes in the cochlea triggered by cytokines, macrophages play an important role in damage and repair processes. Gene set enrichment analysis of the RNA-seq data indicated that the microglia activation-related pathway was triggered at 1 and 15 days after kanamycin administration (Fig. 6a). The recruitment and activation of macrophages prompt the release of cytokines, including interferon γ, TNF, IL-1, IL-6, IL-8, and IL-12, which further exacerbated neuroinflammation in the SGNs following kanamycin exposure. Furthermore, we noted a close association between pyroptosis- and macrophage-related genes, as revealed by protein–protein interaction network analysis (Fig. 6b). Finally, macrophage-related genes such as *Cx3cr1* (also known as CX3C chemokine receptor 1), *Cd68* (a heavily glycosylated glycoprotein highly expressed in macrophages), *Iba-1* (ionized calcium-binding adapter molecule 1, also known as allograft inflammatory factor 1), *Emr1* (EGF-like module-containing mucin-like hormone receptor-like 1, also known as F4/80), and *Itgam* (integrin alpha M, also known as CD11b) were upregulated three-fold compared with Con group SGNs, although no obvious change in *Cx3cl1* (also known as CX3C motif chemokine ligand 1) expression was found (Fig. 6c).

Next, we assessed IBA-1 expression for quantitative and qualitative analysis of macrophages in the SGN region (Fig. 6d). Cochlear cross-sections were used for macrophage analysis. After 5 days, the number of macrophages had increased 1.75-fold compared with the Con group and remained elevated after 30 days; this suggested consistent engraftment during SGN degeneration (Fig. 6e). Whole-mount

preparations confirmed that macrophage expression was increased in both the osseous spiral lamina and SGN regions (Supplementary Fig. S2). As shown in previous studies, activated macrophages were ameboid in shape, unlike inactivated, ramified macrophages [40, 41]. We measured the soma size and length of the branches of each macrophage. Interestingly, the soma area was enlarged (1.78 times larger than that in the Con group) for up to 15 days, while the branches were shorter after 15 days but had recovered by 30 days (Fig. 6e). The engraftment and enlargement of the soma of macrophages indicated macrophage activation in the SGN region during degeneration, similar to previous studies [42-44]. In addition, the macrophages engulfing TuJ positive debris was observed (Supplementary Fig. S3).

SGN degeneration was ameliorated by inhibition of NLRP3 via blockade of the pyroptosis cascade

Mcc950 is a specific inhibitor of the NLRP3 inflammasome that directly targets the ATP-hydrolysis motif without affecting other PRRs such as NLRC4, NLRP1, and AIM2. We applied Mcc950 with kanamycin to inhibit NLRP3 in cochlear organ explants. To assess the integrity of the peripheral neurons, we used antibodies against β-tubulin as a marker of SGNs and their nerve fibers (terminating in HC regions). The loss of the SGN soma area and fibers was largely ameliorated by coadministration of Mcc950 and kanamycin (relative to the major reduction seen in the apical, middle, and basal turns in the group treated with kanamycin alone; Fig. 7a–d). The qRT-PCR results further indicated that the transcripts of *Nlrp3* ($p < 0.001$), *ASC* ($p = 0.012$), *caspase-1* ($p = 0.015$), and *GSDMD* ($p = 0.013$) were markedly decreased by Mcc950 (Fig. 7e), suggesting the inhibition of the NLRP3 inflammasome led to the reduced expression of *caspase-1*. The effector cytokines IL-1β and IL-18 were greatly reduced after NLRP3 inhibition (Fig. 7f). The above results indicate that NLRP3 is an important target for the treatment of SGN degeneration.

Discussion

To the best of our knowledge, this is the first study to describe the roles of pyroptosis and activation of the inflammasome in the SGN degeneration seen in aminoglycoside-induced hearing loss. Our results provide novel insight into the NLRP3 inflammasome activation and increased expression of inflammatory cytokines underlying SGN degeneration, as well as the increased N-GSDMD expression that further exacerbates the damage paralleled with macrophage infiltration (Fig. 8). Moreover, exogenous inhibition of NLRP3 ameliorated SGN damage by blocking pyroptosis and reducing the secretion of cytokines.

The inflammasome is a complex composed of multiple proteins, including NLRP3 as a sensor, ASC as an adaptor, and inflammatory caspases as executioners; these proteins activate GSDMD and pro-inflammatory cytokines including IL-1β and IL-18 and induce cell death in a caspase-1-dependent manner. Assembly and activation of the inflammasome can be triggered by a variety of stimuli. Even small alterations cause a cascade of inflammation via activation of a specific inflammasome pathway via broad downstream responses. Uncontrolled NLRP3 activation can lead to many negative outcomes, including infection, autoimmunity, neurodegeneration, and metabolic disorders [35–38, 45–47]. Tremendous progress in our understanding of the molecular mechanisms of the NLRP3 inflammasome has been made, and the feasibility of pharmacological targeting of NLRP3 to prevent negative disease

states is now clear [39, 48]. Genetic ablation of NLRP3 leads to the same outcomes, which further supports the importance of targeting the inflammasome [49]. In this study, inhibition by Mcc950 treatment reduced SGN degeneration by blocking the release of cytokines and reducing pyroptosis, suggesting the promise of NLRP3 inhibitors for preventing SGN degeneration.

As one of the main resident mononuclear phagocyte populations in the peripheral auditory system, cochlear macrophages are highly reactive to microenvironmental alterations under developmental and pathological conditions. After acoustic trauma and ototoxic drug administration, and in cases of genetic HC lesions, macrophage activation has been observed in the spiral ligament, Rosenthal's canal, and the sensory epithelium [25, 41, 42, 44, 50]. In this study, macrophages were recruited and activated after 5 days of kanamycin treatment and exhibited enlarged soma and CD68 expression suggestive of sustained macrophage activation. Although previous studies demonstrated the accumulation of immune cells expressing CD45, EMR1, IBA-1, ITGAM, and CX3CR1 in the cochlea after injury, the underlying mechanism is unclear[40, 51–53]. Dying cells recruit macrophages via the release of several different chemoattractants, including CX3CL1. However, CX3CR1 knockout did not affect the recruitment of macrophages after acoustic or ototoxic exposure, suggesting that fractalkine is not the only "find-me" signal in the cochlea [50]. In this study, CX3CL1 expression was unaffected, indicating that the activation of other genes underlies macrophage recruitment. The release of cytokines was noted in SGNs after aminoglycoside administration, consistent with previous studies [36, 43, 44, 50]. Previous studies also indicated that IL-1β and IL-18 can stimulate macrophages[54–56]. Our data show that inflammasome assembly caused by DAMPs activates pyroptosis and initiates the release of IL-1β and IL-18, which may exacerbate the activation of macrophages and the subsequent damage caused. Further experiments are needed to explore the potential role of macrophages in aminoglycoside-induced SGN regeneration.

Although SGN damage is considered secondary to HC loss caused by ototoxic drugs, as sequela of neurotrophic factor loss, some studies have posited that SGN degeneration is the primary form of damage [15, 18, 19, 21–23, 57–60]. This study provides evidence that pyroptosis persists for at least 1 month in SGNs after kanamycin administration, suggesting that SGN degeneration could occur independently of total loss of IHCs. SGNs showed morphological alterations characteristic of pyroptosis, including cell swelling, a discontinuous cell membrane, and protuberance formation as early as 1 day after the treatment. SGN loss was observed 15 and 30 days after kanamycin administration, with sufficient IHCs surviving to suggest that pyroptosis was the primary form of injury to SGNs.

Controlled cell death processes, such as apoptosis, occur periodically in both healthy and pathological tissues; however, excessive cell death under pathological conditions leads to cellular efflux, sensed as DAMPs by healthy cells[61]. DAMPs are primed by PRRs; activation of the inflammatory cascade leads to pyroptosis and cytokine release and thus to the recruitment of immune cells[62]. The crosstalk seen between apoptosis and pyroptosis requires further study. The recently coined term "PANoptosis" refers to the intricate connections among pyroptosis, apoptosis, and necrosis, in which it is plausible that tissue undergoes different biological processes over time following insult[63]. Obtaining greater insight into this will be important for developing methods to reverse the detrimental effects of primary defense responses.

The NLRP3 inflammasome may serve as a “critical point” in PANoptosis, although more work is needed to verify this.

There were some limitations to this study. First, long-term observation of pyroptosis after SGN damage was lacking, which is important because NLRP3 inflammasome activation and macrophage infiltration persist for more than 1 month after kanamycin administration. Second, in vivo studies of the effect of NLRP3 blockade on inflammasome formation are warranted, as the organ culture system could not precisely replicate the biological processes of the cochlea. The induction of tissue-specific loss of function of NLRP3 is necessary to further explore the function of inflammasome formation after damage. Moreover, the source of macrophages remains to be fully clarified. Further studies should explore how pyroptosis and inflammation crosstalk affects SGN damage and recovery.

Conclusion

We found that activation of the NLRP3 inflammasome led to inflammatory cell death in SGNs; macrophage infiltration and activation occurred, but Mcc950 significantly ameliorated SGN degeneration via blockade of the NLRP3 inflammasome. This is the first report showing that pyroptosis activation and inflammasome assembly are the main mechanisms underlying the SGN degeneration induced by kanamycin. Our results could aid the development of treatments for SGN degeneration targeting NLRP3.

Abbreviations

ABR
Auditory brainstem response
HCs
Hair cells
IHC
Inner hair cell
OHC
Outer hair cell
SGN
Spiral ganglion neuron
OSL
Osseus spiral lamina
H&E staining
Hematoxylin-eosin staining
RNA-seq
RNA-sequencing
GO
Gene ontology
KEGG

Kyoto Encyclopedia of Genes and Genomes
GSEA
Gene Set Enrichment Analysis
TNF
Tumor necrosis factor
IL-1β
Interleukin 1 beta
IL-18
Interleukin 18
ASC
Apoptosis-associated speck-like protein containing a CARD
GSDMD
Gasdermin D
ROS
Reactive oxygen species
PRRs
Pattern recognition receptors
TLRs
Toll-like receptors
NLRP3
NOD-like receptor family pyrin domain containing 3
NLRP1
NOD-like receptor family pyrin domain containing 1
NLRC4
NOD-like receptors family CARD domain-containing protein 4
AIM2
Absent in Melanoma 2

Declarations

Ethics approval

All the animal experimental protocols were performed in accordance with the Guide for the Care and Use of Medical Laboratory Animals issued by the Ministry of Health of China and approved by the Animal Ethics Committee of Shanghai Jiao Tong University Affiliated Sixth People's Hospital.

Consent for publication

Not applicable.

Availability of data and materials

The datasets used and/or analyzed during the current study are available from the corresponding author upon reasonable request.

Competing interests

The authors declare no competing interests.

Fundings

This work was supported by the National Natural Science Foundation of China (Grant No. 81800919, 81974142, 82000993) and the International Cooperation and Exchange of the National Natural Science Foundation of China (Grant No. 81720108010, 82020108008).

Author's contributions

HS, YX, and DY designed experiments; JF, ZL, and ML performed the experiments; JF, YX, CL, and XZ collected the data; JF, YX, KS, and YL analyzed the data; JF, SM, YX, and HS prepared the figures; YX, and JF wrote the paper. All authors read and approved the final manuscript.

Acknowledgments

We thank Dr. Guisheng Zhong's lab and Bio-Electron Microscopy Facility of ShanghaiTech University for their technical assistance with the TEM analyses.

References

1. WHO. World report on hearing. Geneva: World Health Organization. 2021:Licence: CCBY-NC-SA 3.0 IGO.
2. Prayle AP, Jain K, Touw DJ, Koch BC, Knox AJ, Watson A, et al. The pharmacokinetics and toxicity of morning vs. evening tobramycin dosing for pulmonary exacerbations of cystic fibrosis: A randomised comparison. J Cyst Fibros. 2016;15(4):510-7.
3. Sowinski KM, Magner SJ, Lucksiri A, Scott MK, Hamburger RJ, Mueller BA. Influence of hemodialysis on gentamicin pharmacokinetics, removal during hemodialysis, and recommended dosing. Clin J Am Soc Nephrol. 2008;3(2):355-61.
4. WHO. WHO Reports. Global Tuberculosis Control: Surveillance, Planning, Financing. Geneva: World Health Organization. 2005.
5. Gao Z, Chen Y, Guan MX. Mitochondrial DNA mutations associated with aminoglycoside induced ototoxicity. J Otol. 2017;12(1):1-8.
6. Dillard LK, Martinez RX, Perez LL, Fullerton AM, Chadha S, McMahon CM. Prevalence of aminoglycoside-induced hearing loss in drug-resistant tuberculosis patients: A systematic review. J Infect. 2021;83(1):27-36.

7. WHO. Rapid communication: key changes to treatment of drug-resistant tuberculosis. Geneva: World Health Organization; 2019 (WHO/CDS/TB/201926). 2019;Licence: CC BY-NC-SA 3.0 IGO.
8. Lu J, Li Z, Zhu Y, Yang A, Li R, Zheng J, et al. Mitochondrial 12S rRNA variants in 1642 Han Chinese pediatric subjects with aminoglycoside-induced and nonsyndromic hearing loss. Mitochondrion. 2010;10(4):380-90.
9. Usami S, Abe S, Akita J, Namba A, Shinkawa H, Ishii M, et al. Prevalence of mitochondrial gene mutations among hearing impaired patients. J Med Genet. 2000;37(1):38-40.
10. Vandebona H, Mitchell P, Manwaring N, Griffiths K, Gopinath B, Wang JJ, et al. Prevalence of mitochondrial 1555A–>G mutation in adults of European descent. N Engl J Med. 2009;360(6):642-4.
11. Bitner-Glindzicz M, Pembrey M, Duncan A, Heron J, Ring SM, Hall A, et al. Prevalence of mitochondrial 1555A–>G mutation in European children. N Engl J Med. 2009;360(6):640-2.
12. Li Z, Li R, Chen J, Liao Z, Zhu Y, Qian Y, et al. Mutational analysis of the mitochondrial 12S rRNA gene in Chinese pediatric subjects with aminoglycoside-induced and non-syndromic hearing loss. Hum Genet. 2005;117(1):9-15.
13. Maeda Y, Sasaki A, Kasai S, Goto S, Nishio SY, Sawada K, et al. Prevalence of the mitochondrial 1555 A>G and 1494 C>T mutations in a community-dwelling population in Japan. Hum Genome Var. 2020;7:27.
14. Rodriguez-Ballesteros M, Olarte M, Aguirre LA, Galan F, Galan R, Vallejo LA, et al. Molecular and clinical characterisation of three Spanish families with maternally inherited non-syndromic hearing loss caused by the 1494C->T mutation in the mitochondrial 12S rRNA gene. J Med Genet. 2006;43(11):e54.
15. Ramekers D, Klis SFL, Versnel H. Simultaneous rather than retrograde spiral ganglion cell degeneration following ototoxically induced hair cell loss in the guinea pig cochlea. Hear Res. 2020;390:107928.
16. Ye B, Wang Q, Hu H, Shen Y, Fan C, Chen P, et al. Restoring autophagic flux attenuates cochlear spiral ganglion neuron degeneration by promoting TFEB nuclear translocation via inhibiting MTOR. Autophagy. 2019;15(6):998-1016.
17. Nie C, Hu H, Shen C, Ye B, Wu H, Xiang M. Expression of EFR3A in the mouse cochlea during degeneration of spiral ganglion following hair cell loss. PLoS One. 2015;10(1):e0117345.
18. Sone M, Schachern PA, Paparella MM. Loss of spiral ganglion cells as primary manifestation of aminoglycoside ototoxicity. Hear Res. 1998;115(1-2):217-23.
19. Hinojosa R, Lerner SA. Cochlear neural degeneration without hair cell loss in two patients with aminoglycoside ototoxicity. J Infect Dis. 1987;156(3):449-55.
20. Oishi N, Duscha S, Boukari H, Meyer M, Xie J, Wei G, et al. XBP1 mitigates aminoglycoside-induced endoplasmic reticulum stress and neuronal cell death. Cell Death Dis. 2015;6:e1763.
21. Tu Y, Fan G, Sun H, Cai X, Kong W. Endoplasmic reticulum stress is involved in spiral ganglion neuron apoptosis following chronic kanamycin-induced deafness. Biosci Rep. 2019;39(2).

22. McFadden SL, Ding D, Jiang H, Salvi RJ. Time course of efferent fiber and spiral ganglion cell degeneration following complete hair cell loss in the chinchilla. Brain Res. 2004;997(1):40-51.
23. Gao K, Ding D, Sun H, Roth J, Salvi R. Kanamycin Damages Early Postnatal, but Not Adult Spiral Ganglion Neurons. Neurotox Res. 2017;32(4):603-13.
24. Alam SA, Robinson BK, Huang J, Green SH. Prosurvival and proapoptotic intracellular signaling in rat spiral ganglion neurons in vivo after the loss of hair cells. J Comp Neurol. 2007;503(6):832-52.
25. Kaur T, Zamani D, Tong L, Rubel EW, Ohlemiller KK, Hirose K, et al. Fractalkine Signaling Regulates Macrophage Recruitment into the Cochlea and Promotes the Survival of Spiral Ganglion Neurons after Selective Hair Cell Lesion. J Neurosci. 2015;35(45):15050-61.
26. Bae SH, Yoo JE, Choe YH, Kwak SH, Choi JY, Jung J, et al. Neutrophils infiltrate into the spiral ligament but not the stria vascularis in the cochlea during lipopolysaccharide-induced inflammation. Theranostics. 2021;11(6):2522-33.
27. Ladrech S, Mathieu M, Puel JL, Lenoir M. Supporting cells regulate the remodelling of aminoglycoside-injured organ of Corti, through the release of high mobility group box 1. Eur J Neurosci. 2013;38(6):2962-72.
28. Lyu AR, Kim TH, Park SJ, Shin SA, Jeong SH, Yu Y, et al. Mitochondrial Damage and Necroptosis in Aging Cochlea. Int J Mol Sci. 2020;21(7).
29. Paciello F, Pisani A, Rolesi R, Escarrat V, Galli J, Paludetti G, et al. Noise-Induced Cochlear Damage Involves PPAR Down-Regulation through the Interplay between Oxidative Stress and Inflammation. Antioxidants (Basel). 2021;10(8).
30. Zhang N, Cai J, Xu L, Wang H, Liu W. Cisplatin-Induced Stria Vascularis Damage Is Associated with Inflammation and Fibrosis. Neural Plast. 2020;2020:8851525.
31. Brennan MA, Cookson BT. Salmonella induces macrophage death by caspase-1-dependent necrosis. Mol Microbiol. 2000;38(1):31-40.
32. Cookson BT, Brennan MA. Pro-inflammatory programmed cell death. Trends Microbiol. 2001;9(3):113-4.
33. Fink SL, Cookson BT. Caspase-1-dependent pore formation during pyroptosis leads to osmotic lysis of infected host macrophages. Cell Microbiol. 2006;8(11):1812-25.
34. Martinon F, Burns K, Tschopp J. The inflammasome: a molecular platform triggering activation of inflammatory caspases and processing of proIL-beta. Mol Cell. 2002;10(2):417-26.
35. Johann S, Heitzer M, Kanagaratnam M, Goswami A, Rizo T, Weis J, et al. NLRP3 inflammasome is expressed by astrocytes in the SOD1 mouse model of ALS and in human sporadic ALS patients. Glia. 2015;63(12):2260-73.
36. Tan MS, Tan L, Jiang T, Zhu XC, Wang HF, Jia CD, et al. Amyloid-beta induces NLRP1-dependent neuronal pyroptosis in models of Alzheimer's disease. Cell Death Dis. 2014;5:e1382.
37. von Herrmann KM, Salas LA, Martinez EM, Young AL, Howard JM, Feldman MS, et al. NLRP3 expression in mesencephalic neurons and characterization of a rare NLRP3 polymorphism

associated with decreased risk of Parkinson's disease. NPJ Parkinsons Dis. 2018;4:24.

38. Irrera N, Pizzino G, Calo M, Pallio G, Mannino F, Fama F, et al. Lack of the Nlrp3 Inflammasome Improves Mice Recovery Following Traumatic Brain Injury. Front Pharmacol. 2017;8:459.
39. Ismael S, Nasoohi S, Ishrat T. MCC950, the Selective Inhibitor of Nucleotide Oligomerization Domain-Like Receptor Protein-3 Inflammasome, Protects Mice against Traumatic Brain Injury. J Neurotrauma. 2018;35(11):1294-303.
40. Sun S, Yu H, Yu H, Honglin M, Ni W, Zhang Y, et al. Inhibition of the activation and recruitment of microglia-like cells protects against neomycin-induced ototoxicity. Mol Neurobiol. 2015;51(1):252-67.
41. Brown LN, Xing Y, Noble KV, Barth JL, Panganiban CH, Smythe NM, et al. Macrophage-Mediated Glial Cell Elimination in the Postnatal Mouse Cochlea. Front Mol Neurosci. 2017;10:407.
42. Tan WJ, Thorne PR, Vlajkovic SM. Characterisation of cochlear inflammation in mice following acute and chronic noise exposure. Histochem Cell Biol. 2016;146(2):219-30.
43. Fujioka M, Kanzaki S, Okano HJ, Masuda M, Ogawa K, Okano H. Proinflammatory cytokines expression in noise-induced damaged cochlea. J Neurosci Res. 2006;83(4):575-83.
44. Tornabene SV, Sato K, Pham L, Billings P, Keithley EM. Immune cell recruitment following acoustic trauma. Hear Res. 2006;222(1-2):115-24.
45. Vandanmagsar B, Youm YH, Ravussin A, Galgani JE, Stadler K, Mynatt RL, et al. The NLRP3 inflammasome instigates obesity-induced inflammation and insulin resistance. Nat Med. 2011;17(2):179-88.
46. Hu C, Ding H, Li Y, Pearson JA, Zhang X, Flavell RA, et al. NLRP3 deficiency protects from type 1 diabetes through the regulation of chemotaxis into the pancreatic islets. Proc Natl Acad Sci U S A. 2015;112(36):11318-23.
47. Han X, Sun S, Sun Y, Song Q, Zhu J, Song N, et al. Small molecule-driven NLRP3 inflammation inhibition via interplay between ubiquitination and autophagy: implications for Parkinson disease. Autophagy. 2019;15(11):1860-81.
48. Vande Walle L, Van Opdenbosch N, Jacques P, Fossoul A, Verheugen E, Vogel P, et al. Negative regulation of the NLRP3 inflammasome by A20 protects against arthritis. Nature. 2014;512(7512):69-73.
49. Mangan MSJ, Olhava EJ, Roush WR, Seidel HM, Glick GD, Latz E. Targeting the NLRP3 inflammasome in inflammatory diseases. Nat Rev Drug Discov. 2018;17(8):588-606.
50. Kaur T, Ohlemiller KK, Warchol ME. Genetic disruption of fractalkine signaling leads to enhanced loss of cochlear afferents following ototoxic or acoustic injury. J Comp Neurol. 2018;526(5):824-35.
51. Zhang C, Frye MD, Riordan J, Sharma A, Manohar S, Salvi R, et al. Loss of CX3CR1 augments neutrophil infiltration into cochlear tissues after acoustic overstimulation. J Neurosci Res. 2021.
52. Mizushima Y, Fujimoto C, Kashio A, Kondo K, Yamasoba T. Macrophage recruitment, but not interleukin 1 beta activation, enhances noise-induced hearing damage. Biochem Biophys Res Commun. 2017;493(2):894-900.

53. Wood MB, Zuo J. The Contribution of Immune Infiltrates to Ototoxicity and Cochlear Hair Cell Loss. Front Cell Neurosci. 2017;11:106.
54. Liu C, Chen J, Liu B, Yuan S, Shou D, Wen L, et al. Role of IL-18 in transplant biology. Eur Cytokine Netw. 2018;29(2):48-51.
55. Kaplanski G. Interleukin-18: Biological properties and role in disease pathogenesis. Immunol Rev. 2018;281(1):138-53.
56. Shimodaira T, Matsuda K, Uchibori T, Sugano M, Uehara T, Honda T. Upregulation of osteopontin expression via the interaction of macrophages and fibroblasts under IL-1b stimulation. Cytokine. 2018;110:63-9.
57. Ding D, Jiang H, Salvi RJ. Mechanisms of rapid sensory hair-cell death following co-administration of gentamicin and ethacrynic acid. Hear Res. 2010;259(1-2):16-23.
58. Gao S, Cheng C, Wang M, Jiang P, Zhang L, Wang Y, et al. Blebbistatin Inhibits Neomycin-Induced Apoptosis in Hair Cell-Like HEI-OC-1 Cells and in Cochlear Hair Cells. Front Cell Neurosci. 2019;13:590.
59. Wise AK, Pujol R, Landry TG, Fallon JB, Shepherd RK. Structural and Ultrastructural Changes to Type I Spiral Ganglion Neurons and Schwann Cells in the Deafened Guinea Pig Cochlea. J Assoc Res Otolaryngol. 2017;18(6):751-69.
60. Dodson HC. Loss and survival of spiral ganglion neurons in the guinea pig after intracochlear perfusion with aminoglycosides. J Neurocytol. 1997;26(8):541-56.
61. Alam A, Thelin EP, Tajsic T, Khan DZ, Khellaf A, Patani R, et al. Cellular infiltration in traumatic brain injury. J Neuroinflammation. 2020;17(1):328.
62. Govindarajan V, de Rivero Vaccari JP, Keane RW. Role of inflammasomes in multiple sclerosis and their potential as therapeutic targets. J Neuroinflammation. 2020;17(1):260.
63. Christgen S, Tweedell RE, Kanneganti TD. Programming inflammatory cell death for therapy. Pharmacol Ther. 2021:108010.

Tables

Table1. Primers used for qRT-PCR

Target Genes	Forward Primer (5′ to 3′)	Reverse Primer (5′ to 3′)
Nlrp3	ATTACCCGCCCGAGAAAGG	TCGCAGCAAAGATCCACACAG
ASC	CTTGTCAGGGGATGAACTCAAAA	GCCATACGACTCCAGATAGTAGC
Caspase-1	ACAAGGCACGGGACCTATG	TCCCAGTCAGTCCTGGAAATG
Gsdmd	CCATCGGCCTTTGAGAAAGTG	ACACATGAATAACGGGGTTTCC
IL-1β	GCAACTGTTCCTGAACTCAACT	ATCTTTTGGGGTCCGTCAACT
IL-18	GACTCTTGCGTCAACTTCAAGG	CAGGCTGTCTTTTGTCAACGA
Cd68	GGGGCTCTTGGGAACTACAC	GTACCGTCACAACCTCCCTG
Aif1	ATCAACAAGCAATTCCTCGATGA	CAGCATTCGCTTCAAGGACATA
Itgam	ATGGACGCTGATGGCAATACC	TCCCCATTCACGTCTCCCA
Emr1	TGACTCACCTTGTGGTCCTAA	CTTCCCAGAATCCAGTCTTTCC
Cx3cr1	GAGTATGACGATTCTGCTGAGG	CAGACCGAACGTGAAGACGAG
Cx3cl1	ACGAAATGCGAAATCATGTGC	CTGTGTCGTCTCCAGGACAA
Tlr2	AGCCCATTGAGAGGAAAGCC	CCAAAACACTTCCTGCTGGC
Myd88	CATACCCTTGGTCGCGCTTA	CCAGGCATCCAACAAACTGC
Gapdh	TGTGTCCGTCGTGGATCTGA	CCTGCTTCACCACCTTCTTGA

Figures

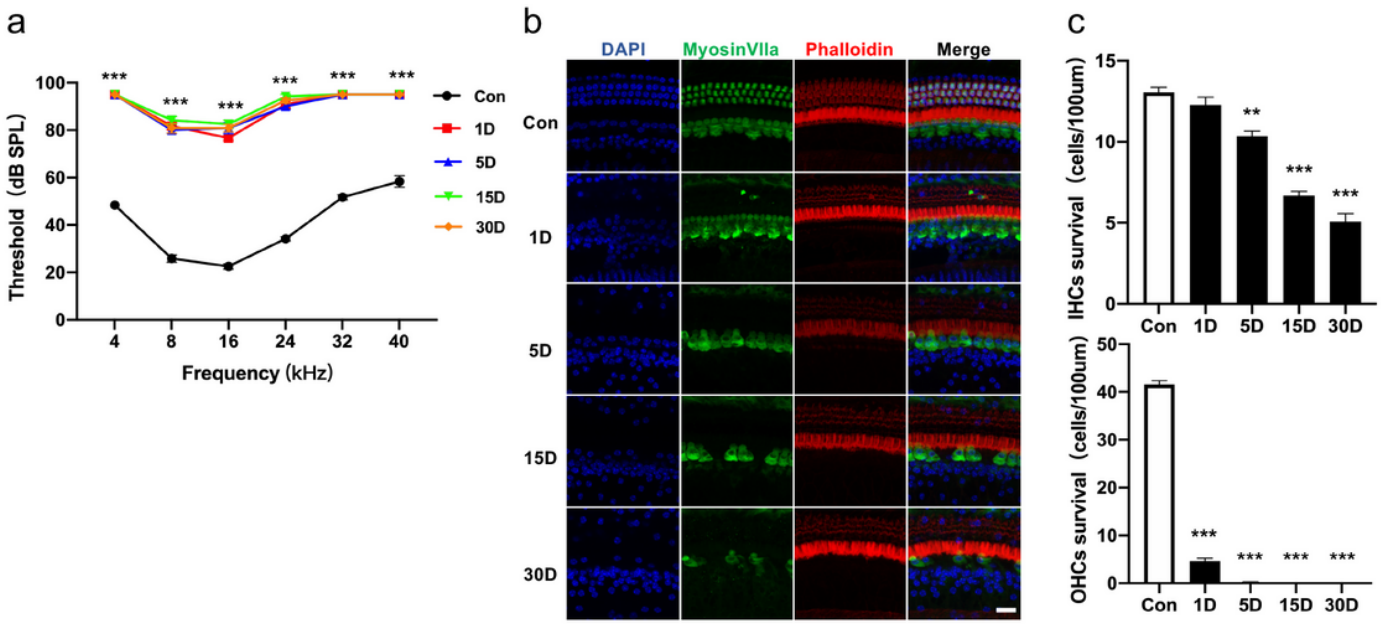

Figure 1

Cochlear hair cell (HC) damage by kanamycin and furosemide administration. (a) The auditory brainstem response (ABR) threshold increased after kanamycin treatment (n = 6). (b) Representative morphological changes in HCs of the middle turn in the control (Con) and experimental groups. (c) Quantification of inner hair cells (IHCs) and outer hair cells (OHCs) in the middle turn (n = 3). Data are means ± standard error of the mean (SEM). *$p < 0.05$; **$p < 0.01$; ***$p < 0.001$. Scale bar, 20 μm.

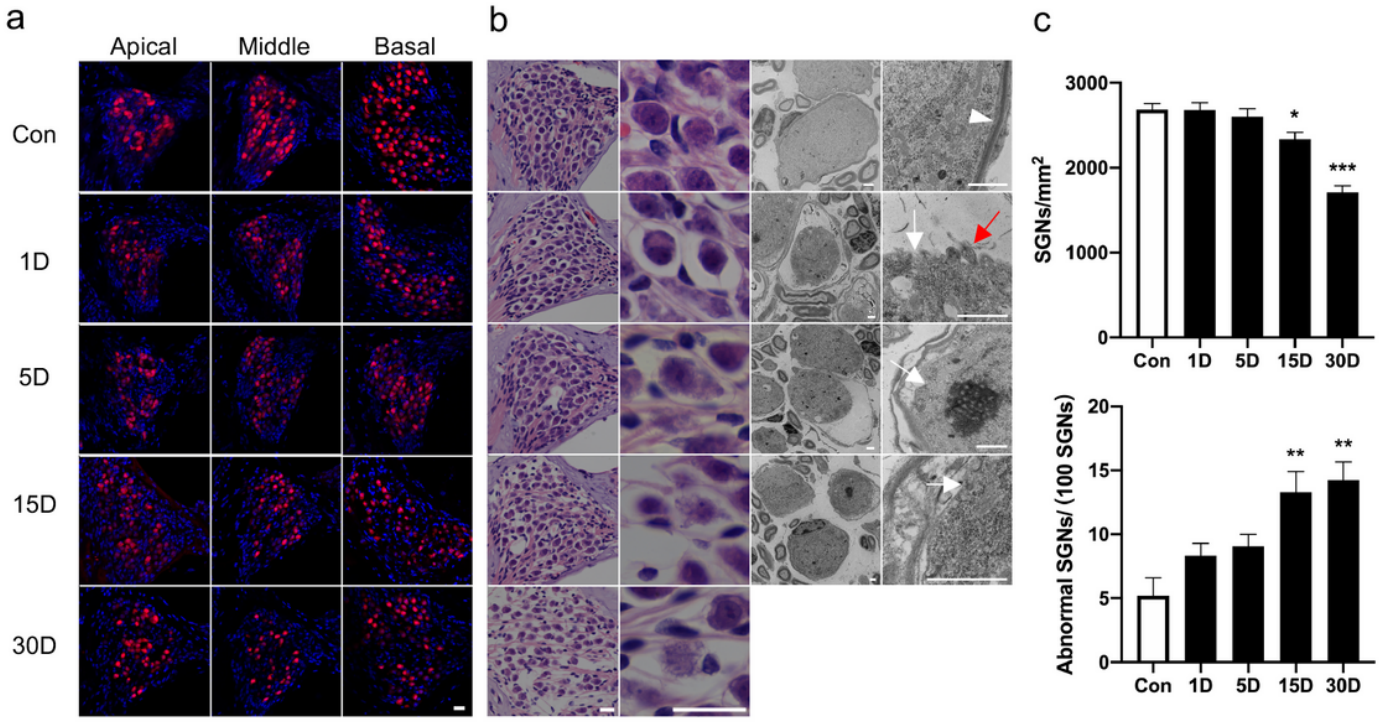

Figure 2

Degeneration of spiral ganglion neurons (SGNs). (a) NeuN staining (red) showing a marked decrease in SGNs in the apical, middle, and basal turns after kanamycin administration. Scale bar, 20 μm. (b) Hematoxylin and eosin (H&E) staining and transmission electron microscopy (TEM) images of middle turns in the various groups. Scale bars, 20 and 1 μm, respectively. The white triangle denotes the intact cell membrane in the Con group, the white arrows indicate the small pores in the cell membrane after treatment, and the red arrow indicates mitochondria overflowing from the cytoplasm. (c) Quantification of normal (upper panel, n = 4–7) and abnormal (lower panel, n = 4–6) SGNs in the middle turn. Abnormal SGNs showed cell swelling and membrane rupture. Data are means ± SEM. *$p < 0.05$; **$p < 0.01$; ***$p < 0.001$.

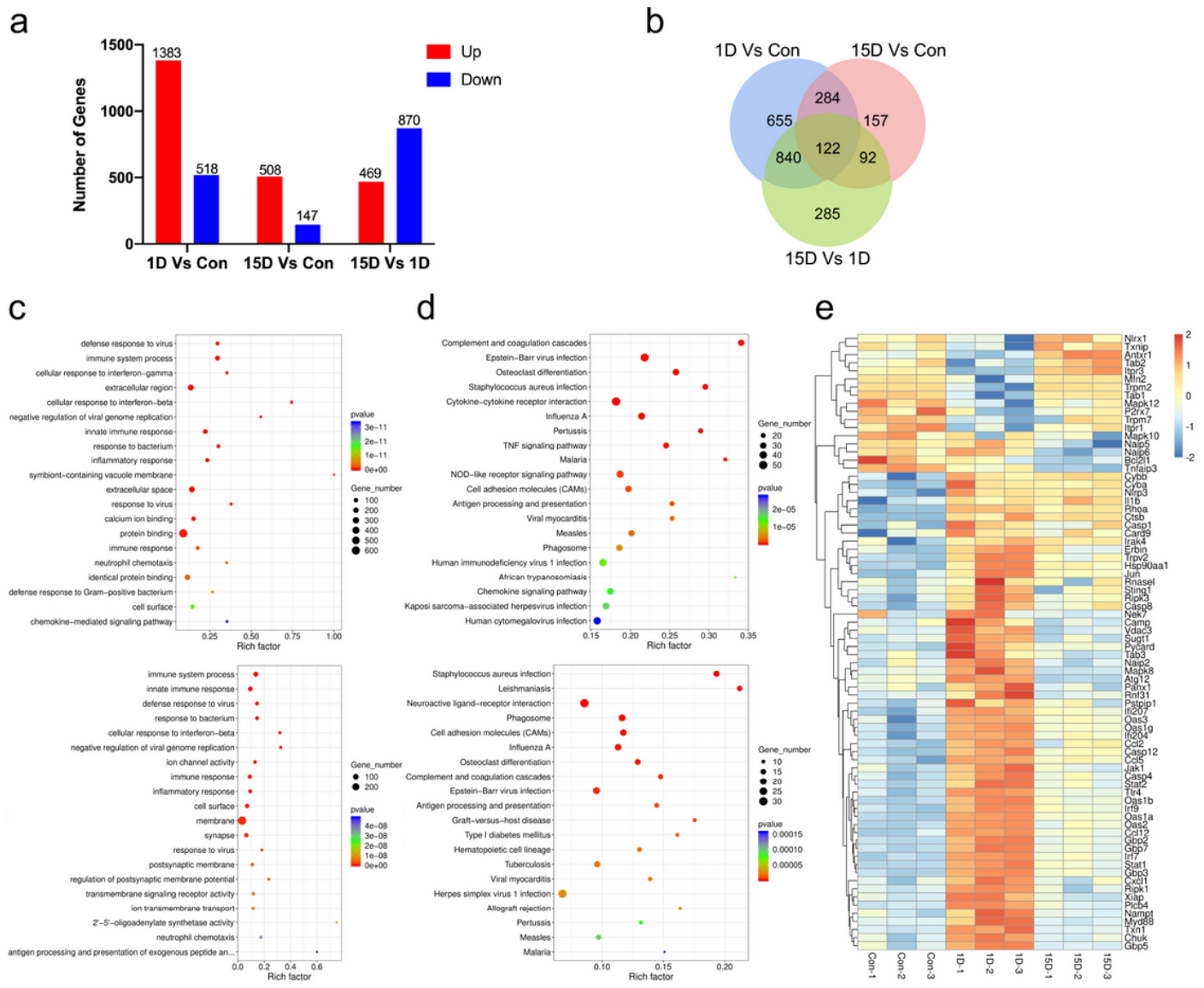

Figure 3

Inflammatory and immune-related responses after kanamycin-induced SGN damage. (a) Bar plot of differentially expressed genes between groups. (b) Venn diagram showing overlapping genes in the 1 D vs. Con, 15 D vs. Con, and 15 D vs. 1 D group comparisons. (c) Results of Gene Ontology (GO) enrichment analysis showing the top 20 pathways in the 1 D vs. Con (upper panel) and 15 D vs. Con (lower panel) group comparisons. (d) Results of Kyoto Encyclopedia of Genes and Genomes (KEGG) enrichment analysis showing the top 20 pathways in the 1 D vs. Con (upper panel) and 15 D vs. Con (lower panel) group comparisons. (e) Heatmap of genes involved in the NOD-like receptor signaling pathway.

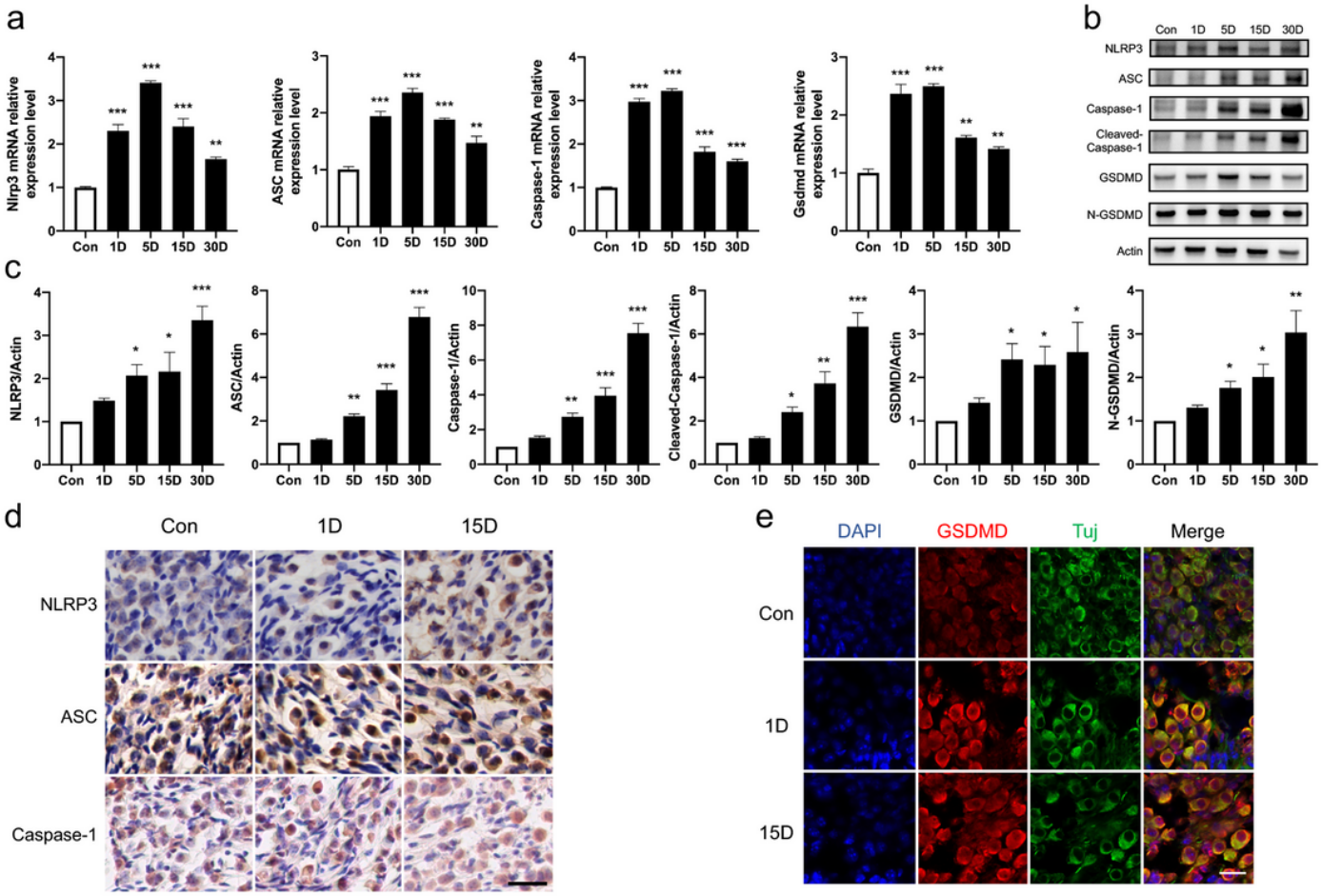

Figure 4

Upregulation of pyroptosis- and inflammasome-related genes associated with SGN degeneration. (a) Quantitative real-time polymerase chain reaction showing that *Nlrp3*, *ASC*, *Casp1*, and *Gsdmd* were significantly upregulated after kanamycin treatment (n = 3). (b) Western blot analysis indicating that upregulated levels of the pyroptosis-related proteins Nlrp3, ASC, caspase-1, cleaved caspase-1, GSDMD, and N-terminal fragment of GSDMD (N-GSDMD) were associated with SGN degeneration. (c) Quantification of NLRP3, ASC, caspase-1, cleaved caspase-1, GSDMD, and N-GSDMD expression (n = 3). (d) Immunohistochemical staining of NLRP3, ASC, and caspase-1 in the middle turn of Rosenthal's canal in Con, 1 D, and 15 D animals. Scale bar, 25 μm. (e) Immunofluorescence staining showing that GSDMD expression was increased, especially around cell membranes after 1 and 15 days. Scale bar, 20 μm. The data are means ± SEM. *$p < 0.05$; **$p < 0.01$; ***$p < 0.001$.

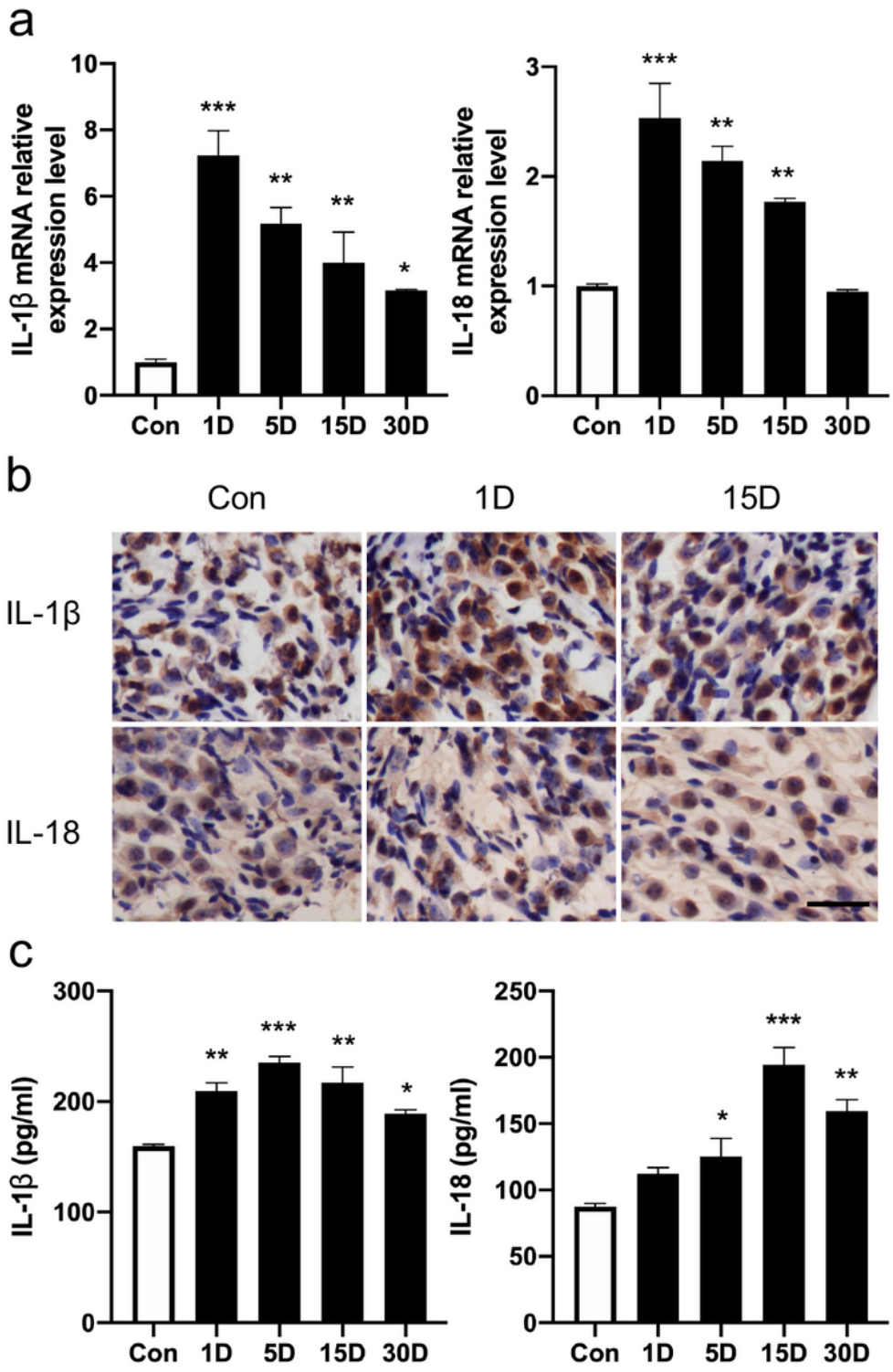

Figure 5

Increased release of interleukin (IL)-1β and IL-18 contributing to neuroinflammation. (a) mRNA levels of IL-1β and IL-18 in SGN regions after kanamycin injection (n = 3). (b) Immunohistochemical staining of IL-1β and IL-18 in the middle turn of Rosenthal's canal from the Con, 1 D, and 15 D groups. Scale bar, 25 μm. (c) Enzyme-linked immunosorbent assay (ELISA) for IL-1β and IL-18 after kanamycin injection (n = 3). Data are means ± SEM. *$p < 0.05$; **$p < 0.01$; ***$p < 0.001$.

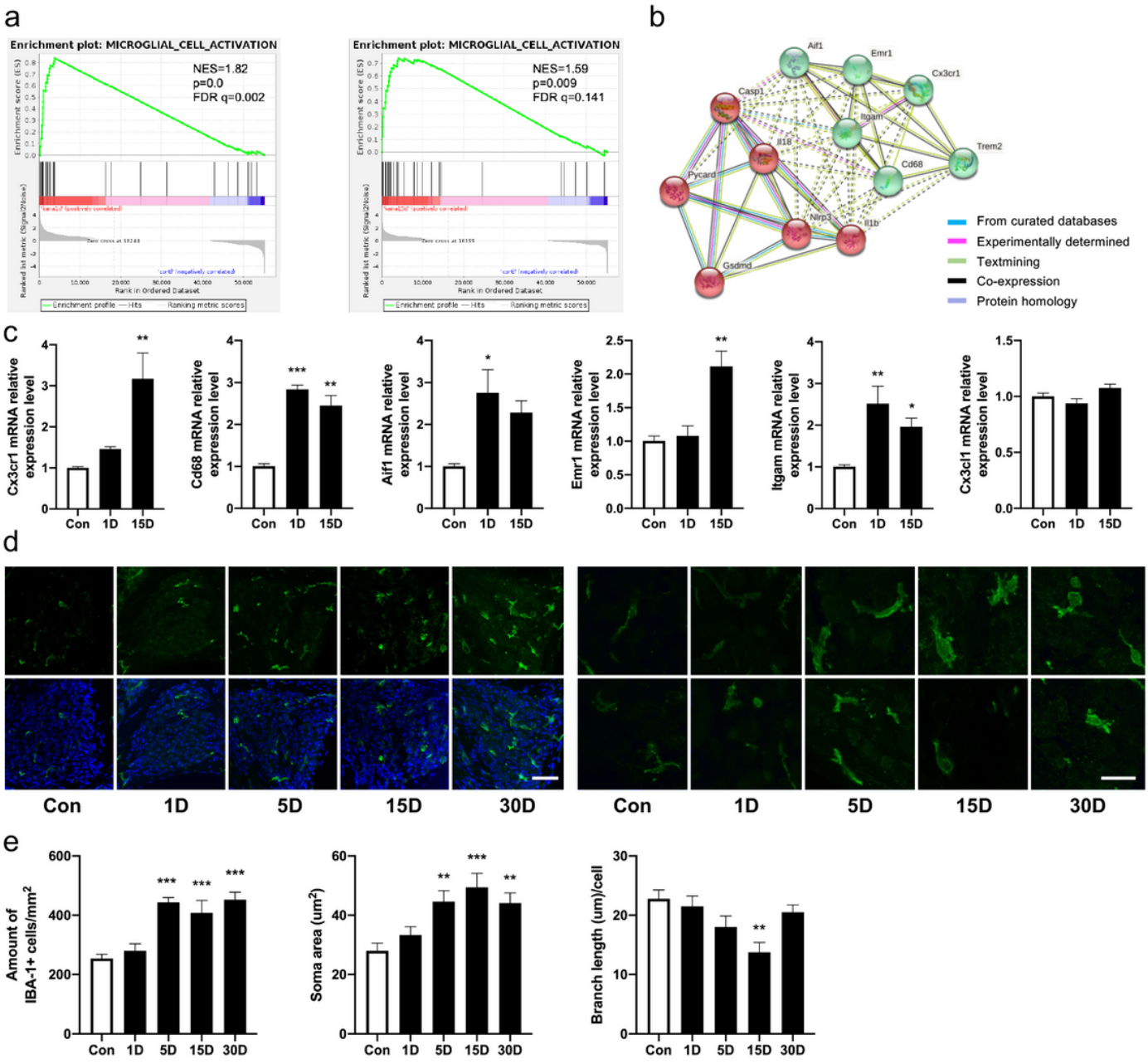

Figure 6

Macrophage recruitment and activation in the SGN region after kanamycin treatment. (a) Enrichment plot of microglial cell activation in the 1 D vs. Con (left panel) and 15 D vs. Con (right panel) group comparisons. NES, normalized enrichment score. FDR, false discovery rate. (b) Protein–protein interactions between pyroptosis- and macrophage-related genes. (c) Relative mRNA expression levels of the macrophage activation-related genes *Cx3cr1, Cd68, Iba-1, Emr1*, *Itgam*, and *Cx3cl1* (n = 3–4). (d) IBA-1-positive macrophages in the middle turn of Rosenthal's canal under low (left panel) and high (right panel) magnification. Scale bar in the left panel, 50 μm. Scale bar in the right panel, 20 μm. (g) Average number of IBA1-positive cells in the middle turn of Rosenthal's canal (n = 3) and the soma area (n = 20–24) and branch length (n = 16) of IBA1-positive cells. Data are means ± SEM. *$p < 0.05$; **$p < 0.01$; ***$p < 0.001$.

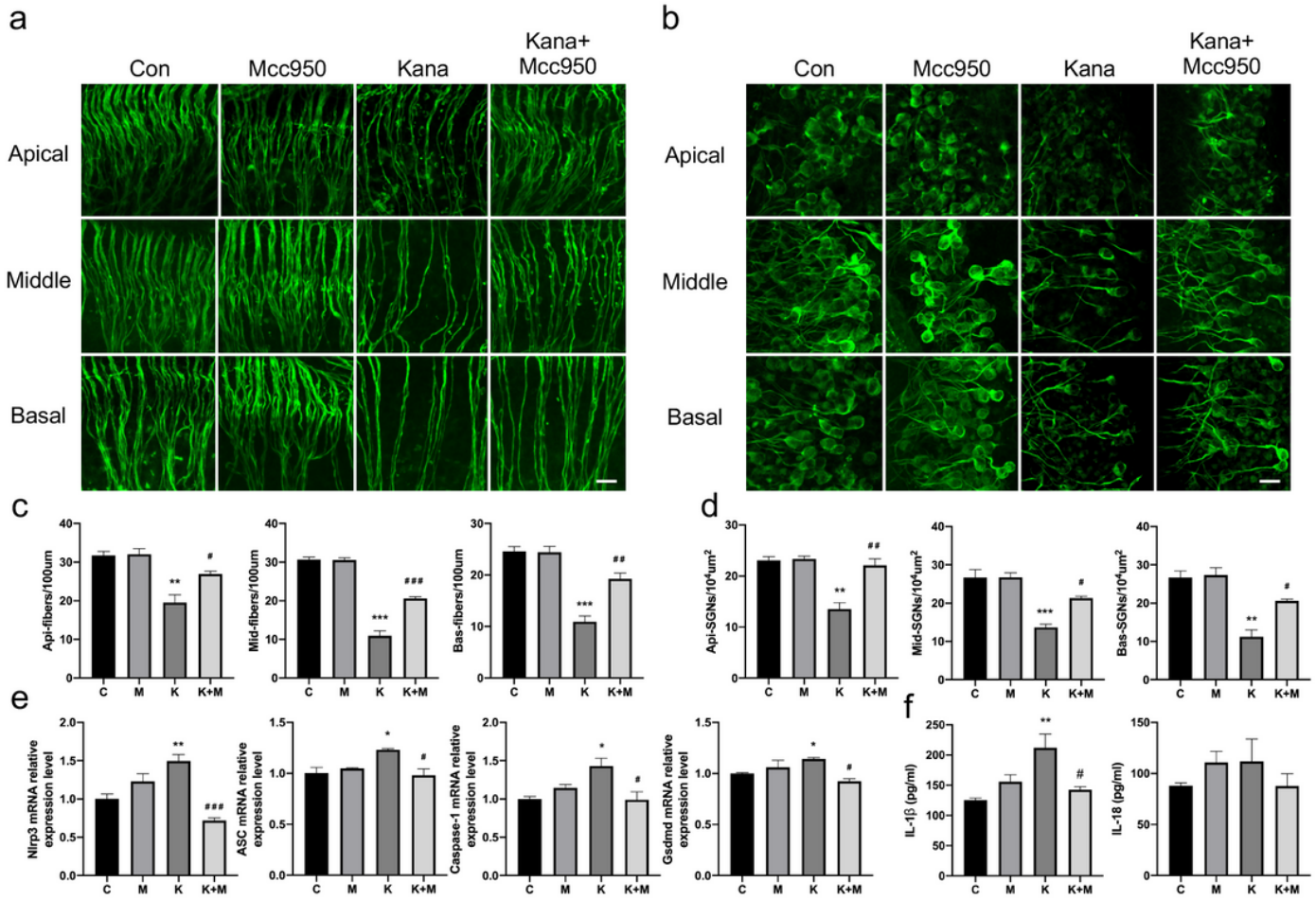

Figure 7

SGN protection and reduced expression of pyroptosis-related molecules after NLRP3 inflammasome inhibition. (a) SGN fibers (green) in the apical, middle, and basal turns. (b) SGN somas in the apical, middle, and basal turns. (c) Quantification of SGN fibers in the four groups (all n = 3). (d) Quantification of SGNs in the four groups (n = 3). (e) Relative mRNA expression levels of *Nlrp3*, *ASC*, *Caspase*-1, and *Gsdmd* (n = 3). (f) ELISA for IL-1β and IL-18 (n = 3). Data are means ± SEM. C, Con group; M, Mcc950 group; K, kanamycin group; K+M, kanamycin plus Mcc950 group. Asterisk (*) denotes statistical analysis between Kanamycin and Control groups, *$p < 0.05$; **$p < 0.01$; ***$p < 0.001$. Pound (#) denotes statistical analysis between Kanamycin plus Mcc950 and Kanamycin groups, #$p < 0.05$; ##$p < 0.01$; ###$p < 0.001$. Scale bar, 20 μm.

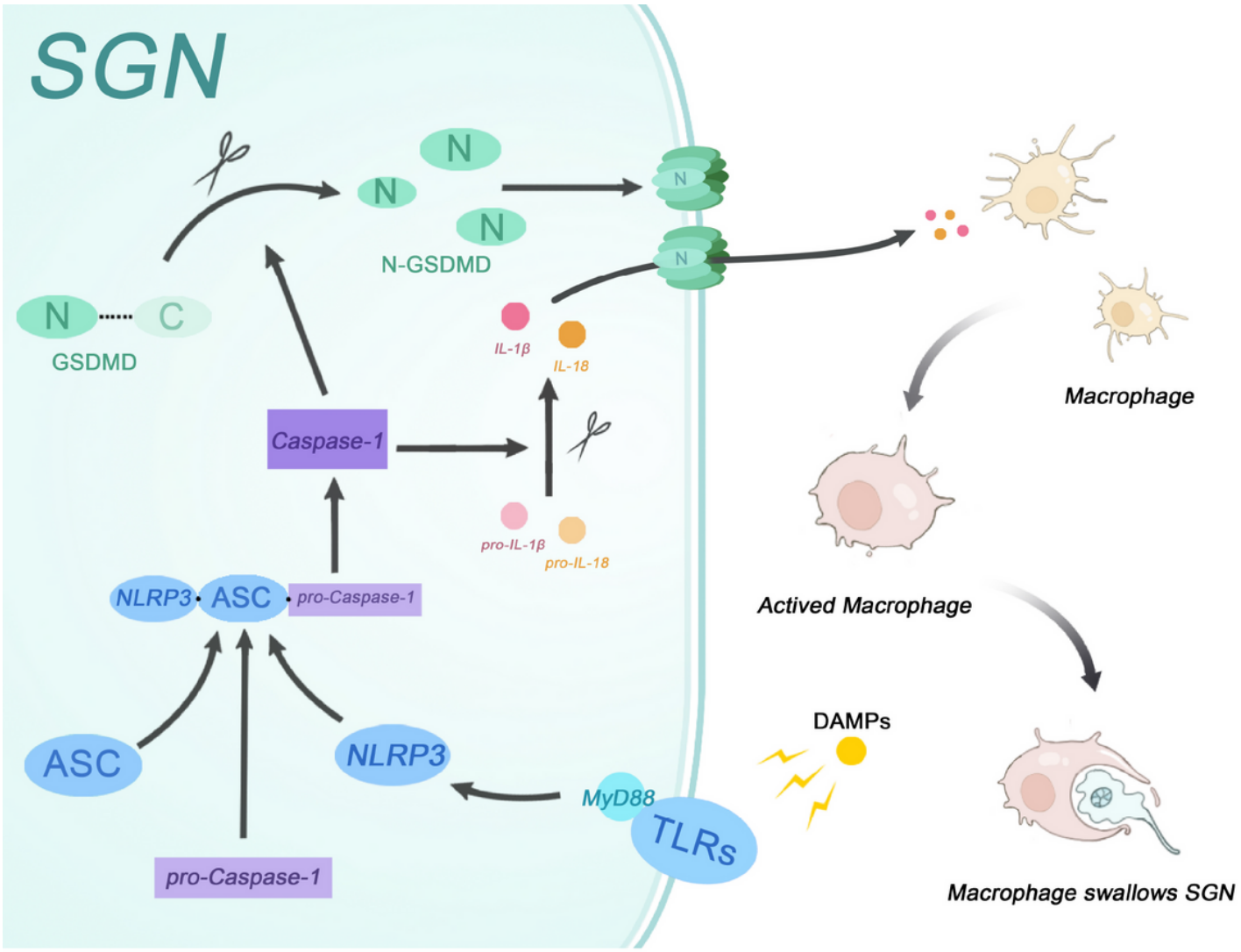

Figure 8

Schematic of NLRP3 inflammasome and macrophage activation in SGNs. Kanamycin-induced damage-associated molecular patterns (DAMPs) activated the NLRP3 inflammasome; caspase-1 was then recruited to cleave the GSDMD protein to the N-GSDMD, which forms small pores in the plasma membrane. Meanwhile, the cytokines IL-1β and IL-18 were cleaved and released into the extracellular spaces by caspase-1, thereby exacerbating neuroinflammation. The macrophages were recruited and activated in the SGN region after kanamycin administration.

Supplementary Files

This is a list of supplementary files associated with this preprint. Click to download.

- Additionalfile.pdf